Influence of the Anodic Work Function on the Performance of Organic Solar Cells

Holger Frohne,[a] Sean E. Shaheen,[b]
Christoph J. Brabec,[c] David C. Müller,[a]
N. Serdar Sariciftci,[b] and Klaus Meerholz*[a]

KEYWORDS:

conducting polymers · organic solar cells · PEDOT · photovoltaic cells · variable work function

Organic solar cells (OSCs) based on conjugated polymer – fullerene blends—so-called "bulk heterojunction" solar cells—are a promising approach to inexpensive solar energy conversion for all kinds of portable applications.[1–3] The general device geometry consists of a multilayer stack of transparent conducting oxide/polymeric contact/photoactive donor--acceptor blend/metal. The driving force for the generation and transport of charges in polymeric OSCs is the built-in potential V_{bi}.[4] For MIM (metal/insulator/metal) type devices, the built-in potential results from the disparate work functions ϕ_w of the two contact materials. In a zero-order approximation, the magnitude of V_{bi} is equal to the difference in ϕ_w between the two contacts $\Delta\phi_w$, assuming there are no dipoles present at the metal/organic interfaces due to, for example, interfacial chemistry.[5, 6]

Throughout the OSC literature, V_{bi} is commonly estimated by measuring the open-circuit voltage V_{oc} (where the overall device current is zero) for various incident light intensities. For a sufficiently large incident intensity P_{min}, V_{oc} approaches a saturation level and $V_{oc} \approx V_{bi}$. Generally it is also expected that the current vanishes at $U = V_{bi}$ (since $J = 0 @ V_{oc}$). This presumes that injection of carriers from the electrodes is negligible. Whenever this is not the case, the net photocurrent (the difference of photocurrent and dark current) has to be

[a] Prof. Dr. K. Meerholz,[+] H. Frohne,[+] D. C. Müller[+]
Chemistry Department and Center for Nanoscience (CeNS)
Universität München
Butenandtstrasse 11, 81377 München (Germany)
E-mail: klaus.meerholz@uni-koeln.de

[b] Dr. S. E. Shaheen,[++] Prof. Dr. N. S. Sariciftci
Linzer Institut für organische Solarzellen (LIOS)
Physikalische Chemie
Johannes Kepler Universität Linz
Altenbergerstrasse 69, 4040 Linz (Austria)

[c] Dr. C. J. Brabec
Siemens AG CT
MM1 "Innovative Polymers"
Paul-Gossen-Strasse 100, 91052 Erlangen (Germany)

[+] New address:
Institut für Physikalische Chemie
Universität zu Köln
Luxemburgerstrasse 116, 50939 Köln (Germany)
Fax: (+ 49) 221 470 5144

[++] New address:
National Renewable Energy Laboratory
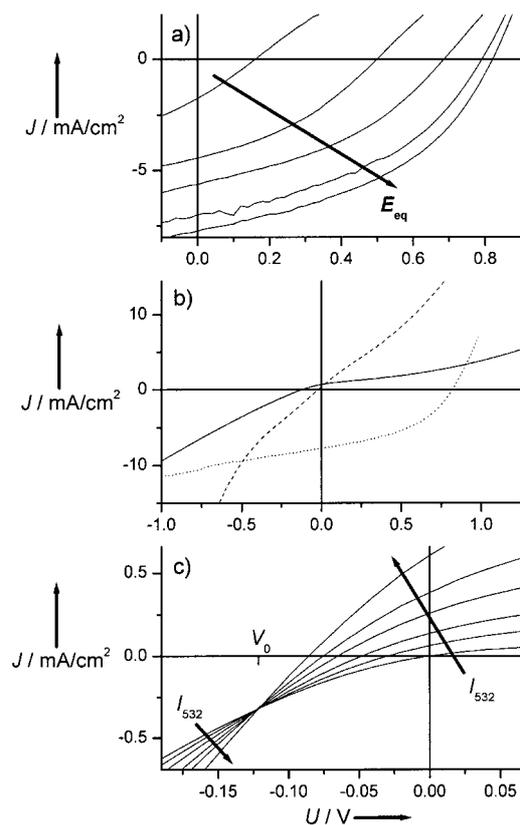1617 Cole Blvd., MS 3211 Golden, CO 80401 (USA)

considered, yielding the compensation voltage V_0 ($= V_{bi}$).[7] As a result of the occurrence of a dark current, V_{oc} can be significantly smaller than V_{bi}.

Thus, the contact materials are among the key parameters to altering the performance of an OSC in general. In the case of metal/conjugated polymer – fullerene blend/metal devices, which are among the most efficient OSCs known to date, it has been demonstrated that the open-circuit voltage V_{oc} depends linearly on the electrochemical reduction potential of the fullerene in solution, namely its acceptor strength. By contrast, the alteration of the metal contact (cathode) had little effect on the device performance.[4, 8] Thus, it was concluded that the value of ϕ_w of the thermally evaporated metal contact becomes pinned to the electron acceptor energy level (LUMO) of the fullerene.[9]

A material commonly chosen as the polymeric contact (anode) is poly(3,4-ethylenedioxythiophene) (PEDOT) doped with poly-(styrenesulfonate) (PSS). We have recently demonstrated that its work function can be conveniently altered electrochemically.[10, 11] We use this technique in this paper to systematically study the influence of V_{bi} in ITO/PEDOT(E_{eq})/photoactive donor – acceptor blend/Al devices. PEDOT was polymerized electrochemically on indium tin oxide (ITO) as a transparent electrode. In a second step it was electrochemically adjusted ex situ to the desired equilibrium potential E_{eq}.[10, 11] A blend of the soluble fullerene derivative PCBM ([6,6]-phenyl C_{61}-butyric acid methyl ester; acceptor) and MDMO-PPV (poly(2-methoxy-5-(3′,7′-dimethyloctyloxy)-para-phenylene vinylene; donor) was spin-cast as the photoactive material, and finally the aluminum contact was evaporated (for details see Experimental Section).

Figure 1 shows the current – potential ($J – V$) curves of our OSCs with varying PEDOT contacts. The devices were illuminated with a 532 nm laser (intensity $I_0 = 200$ mW cm^{-2}). With decreasing E_{eq} of the PEDOT layer, the open-circuit voltage V_{oc} decreases as well (Figures 1a and 1b). This is expected since the difference in work function between the two contacts $\Delta\phi_w$ ($\approx V_{bi}$) decreases. It was a rather surprising finding that in all devices with low absolute values of $\Delta\phi_w$ there is a voltage at which the current density is independent of the incident light intensity I_0 but has a finite, nonzero value (Figure 1c). Furthermore, in these devices V_{oc} does depend on I_0 under all circumstances unlike in "normal" OSCs. Since the dark current ($I_0 = 0$) also coincides with all other data sets at this point, this clearly indicated that there is a contribution to the overall photocurrent originating from (dark) injection processes rather than from bulk photogeneration. Recognizing that this current contribution plays an important role at least for small $\Delta\phi_w$ values, we adapt the term compensation voltage V_0 as introduced by Wei et al. for the voltage at which the net photocurrent (difference between the photocurrent the dark current) is zero.[12]

Figure 2 shows the dependence of V_0 on E_{eq}. In perfect agreement with our earlier photovoltaic (PV) studies on OLED devices using pristine MDMO-PPV,[5] we found a linear dependence with a slope of 0.8, indicating that the ϕ_w of the PEDOT layer is not pinned to any of the energy levels present within the active layer blend. The PV results deviated from the linear dependence (Figure 2a) whenever E_{eq} of the PEDOT anode

Figure 1. J–V curves of OSC devices of the general structure PEDOT(E$_{eq}$)/ MDMO-PPV:PCBM/Al in dependence of the equilibrium potential E$_{eq}$ of the PEDOT layer. a) E$_{eq}$ of PEDOT layer following the arrow: −0.21 V, −0.01 V, +0.18 V, +0.39 V, and +0.53 V versus Ag/AgCl; I$_0$ = 200 mW cm^{-2} (532 nm). b) E$_{eq}$ of PEDOT layer: −0.81 V ("inverted" OSC; solid line), −0.57 V ("zero-built-in-field" OSC; dashed line), +0.53 V ("normal" OSC; dotted line; see also Figure 1 a); I$_0$ = 200 mW cm^{-2} (532 nm). c) "Inverted" OSC: V$_{bi}$ = −0.12 V; I$_0$ following the arrows: 0 mW cm^{-2}, 45 mW cm^{-2}, 70 mW cm^{-2}, 120 mW cm^{-2}, 200 mW cm^{-2}, and 330 mW cm^{-2} (532 nm).

approached or even exceeded the oxidation potential E_{ox} of MDMO-PPV, as determined by cyclic voltammetry in solution (Figure 2 c). We attribute this to redox chemistry between the MDMO-PPV and the highly oxidized PEDOT layer (see below). Because of these redox reactions, the range $E_{eq} > E_{ox}$ is "forbidden" (shaded area in Figure 2 a). On the other hand, passing the reduction potential of PCBM (Figure 2 d) does not seem to harm V_0. This finding can be explained in terms of missing redox states for completely dedoped (neutral) PEDOT (compare Figure 2 b) and, therefore, the absence of a sufficient number of counter ions, which are necessary to compensate redox reactions across the interface. We point out that exact correlations between the redox potentials determined in solution (Figures 2 c and 2 d) and the situation in a real device is not possible. However, electrochemical investigations of solid films of the respective materials will be similarly problematic due to slow electron transfer kinetics, generally leading to scan-rate dependent overpotentials.

In Figure 3 the properties of our OSC devices are displayed as a function of the experimentally determined V_0. This is preferable over the ex situ determined E_{eq} as ordinate (used in Figure 2), because V_0 reflects the "real" energetic situation in the devices.
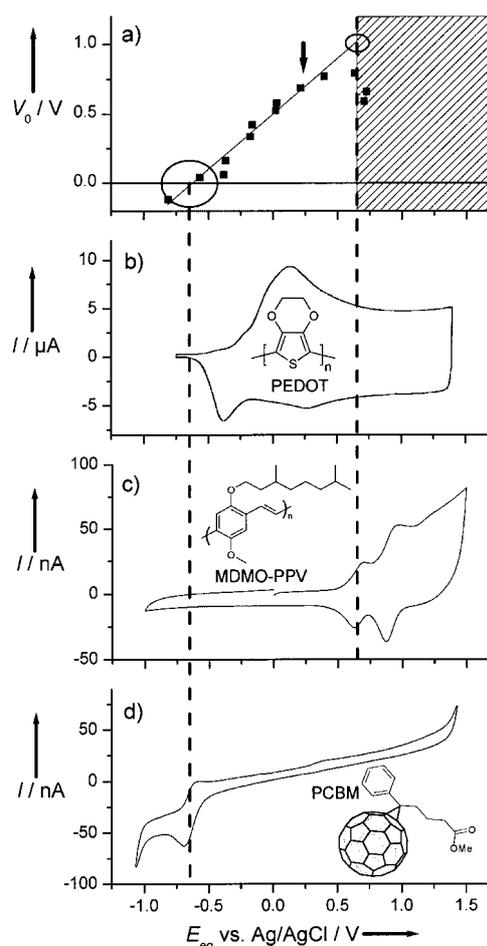

Figure 2. Comparison of OSC device performance with electrochemical properties of involved compounds. a) Compensation voltage V$_0$ in PEDOT(E$_{eq}$)/ MDMO-PPV:PCBM/Al devices as a function of the pre-adjusted E$_{eq}$ of the PEDOT layer. The shaded area indicates the "forbidden" potential range, in which PEDOT is able to oxidize MDMO-PPV (see "doped" OSCs). The arrow indicates the commercial PEDOT. b) Cyclic voltammogram of a PEDOT-film atop the Pt work electrode in acetonitrile with tetrabutylammonium hexafluorophosphate (TBAPF$_6$, 0.1 M). The scan rate was ν = 10 mV s^{-1}. c) Cyclic voltammogram of MDMO-PPV in methylene chloride (MC) with TBAPF$_6$ (0.1 M), ν = 100 mV s^{-1}. The right-hand vertical dashed line indicates the first oxidation potential (defining the beginning of "forbidden" potential range). d) Cyclic voltammogram of PCBM in TBAPF$_6$/MC (0.1 M), ν = 100 mV s^{-1}. The left-hand vertical dashed line indicates the first reduction potential.

For $V_0 = 0$ V, all characteristic device parameters are zero, as expected due to the missing driving force for transportation of photogenerated charge carriers.

Both the absolute short-circuit current J_{sc} ($U = 0$ V; all dark contributions vanish) and the fill factor FF increase monotonously with increasing V_0 (Figures 3 a and 3 b). By contrast, the energy conversion efficiency η_{conv} (Figure 3 c) remains negligibly small for $V_0 < 0.3$ V and only then increases, reaching a maximum of about 2% shortly before reaching the "forbidden" potential range. The origin behind the onset behavior seems to be related to the absence ($V_0 > 0.3$ V) or presence ($V_0 < 0.3$ V) of injection currents (Figure 1 c) in the devices. Any such light-independent contribution to the overall current will reduce the devices efficiency (see below). Furthermore, it is well known that for low
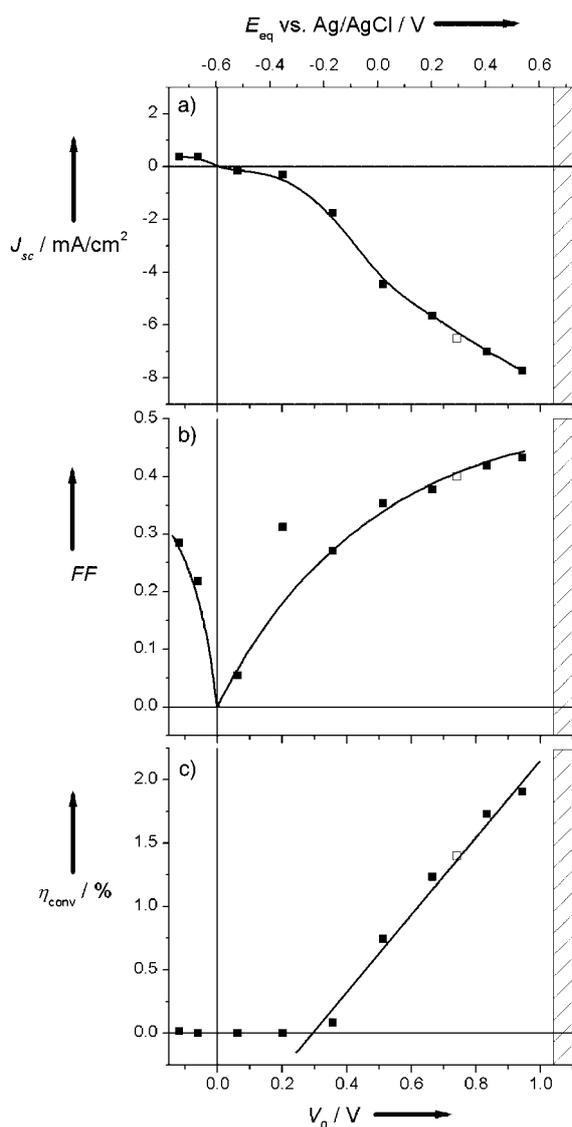
Figure 3. Dependence of OSC properties on the compensation voltage V_0 (bottom axis) and E_{eq} (top axis), respectively, in OSC devices of the general structure PEDOT(E_{eq})/MDMO-PPV:PCBM/Al ($I_0 = 200\ mW\,cm^{-2}@532\ nm$). The lines are guides to the eye. a) Short circuit current density J_{sc}. b) Fill factor FF. c) Energy conversion efficiency η_{conv}. The open symbols refer to the reference device using commercial PEDOT as the anode. All other lines are guide to the eye. The shaded area indicates the "forbidden" potential range (see "doped" OSC).

injection barriers (Ohmic contacts) an accumulation region of free charge carriers is established close to the contact, resulting in band bending. This leads to a reduction of the internal electric field in the device by about 0.2 V.

The reference device using a commercial PEDOT anode yields $V_{oc} = 0.74$ V, $J_{sc} = 6.5$ mA cm^{-2} (200 mW cm^{-2}@532 nm), $FF = 0.4$, and $\eta = 1.4\%$. A true comparison of our data with earlier results by Shaheen et al.[3] is difficult due to the following reasons: 1) we used monochromatic illumination (laser 532 nm) while Shaheen et al. used a white-light illumination (AM1.5); 2) the morphology of the PEDOT as well as the photoactive layers might be different; 3) the device used by Shaheen et al. comprised a thin LiF layer at the cathode side, which is known to increase the built-in potential of the devices. In any case, there is clear

potential on improving our devices relative to those using commercial PEDOT. When extrapolating that data to $E_{eq} = E_{ox,PPV}$ we obtain $V_{oc} \approx 1.0$ V, $J_{sc} \approx 8$ mA cm^{-2}, $FF \approx 0.44$, and $\eta \approx 2\%$, a substantial overall improvement over the reference. Katz et al. had reported $V_{oc} \approx 1.2$ V for temperatures below 200 K.[14] We attribute the difference to the disparate temperature at which the experiments were performed (room temperature here versus liquid helium conditions in ref. [14]).

In the following we will discuss four situations in more detail: For reasons of completeness we start with "normal" OSCs exhibiting relatively large open-circuit voltages and short-circuit currents (type 1). This is followed by two novel device types, namely "zero built-in field" OSCs (type 2) and "inverted" OSCs (type 3). Finally, we discuss "doped" OSCs (type 4). Except for type 1 devices, all others are devices of limited practical use, however, of great scientific interest for the understanding of the underlying physics of OSCs.

1) "Normal" OSCs: Such devices ($V_{bi} \gg 0$) are commonly achieved using a highly doped PEDOT layer as the polymeric contact, for example by using commercial PEDOT (see arrow in Figure 2a and open symbols in Figure 3). Due to the relatively large difference in work functions of the two contacts (Figure 4Ia) "normal" OSCs exhibit the strongest diode rectification among the devices studied here. The injection current for holes and electrons in the operating range relevant for OSCs ($U < V_0$) is negligible due to the tilt of the levels in the unfavorable direction (see Figure 4Ic). Therefore, in these devices we can assume $V_0 \approx V_{oc}$.

2) "Zero built-in field" OSCs: The built-in field V_{bi} becomes zero when E_{eq} of the PEDOT contact equals the PCBM reduction potential (Figure 2a; $E_{eq} = E_{red,PCBM}$). This finding proves that the pinning of thermally evaporated metal cathodes[9] occurs exactly at the PCBM LUMO level and not below.

"Zero built-in field" OSCs exhibit Ohmic contacts for electrons at both electrodes (see Figure 4II). This has two implications: a) the $J–V$ characteristics are symmetrical for the two bias directions, and b) the dark injection of electrons injected by the PEDOT contact in the forward direction becomes strongest among the series of devices studied here.

3) "Inverted" OSCs: By dedoping the PEDOT layer even past the PCBM acceptor level ($E_{eq} < E_{red,PCBM}$), we achieved devices where J_{sc} and V_0, respectively, have opposite signs compared with "normal" OSCs. This proved that nondoped PEDOT may serve as cathode, unlike in "normal" OSCs or organic light-emitting diodes (OLEDs) where highly doped PEDOT typically serves as the anode.

The "inverted" OSCs have a small internal barrier for photo-generated electrons leaving at the PEDOT contact (see Figure 4IIIb). Therefore, the total current is reduced compared with the "zero built-in field" devices.

Due to the absence of more negative redox states in the PEDOT (Figure 2b), devices with $V_0 < -0.12$ V are experimentally not accessible. However, even if a π-conjugated polymer with such negative redox states existed, we expect "doping problems" similar to those anticipated for high doping levels of the PEDOT (see type 4 devices).

4) "Doped" OSCs: In these devices the PEDOT-layer was preadjusted beyond the oxidation potential of the MDMO-PPV
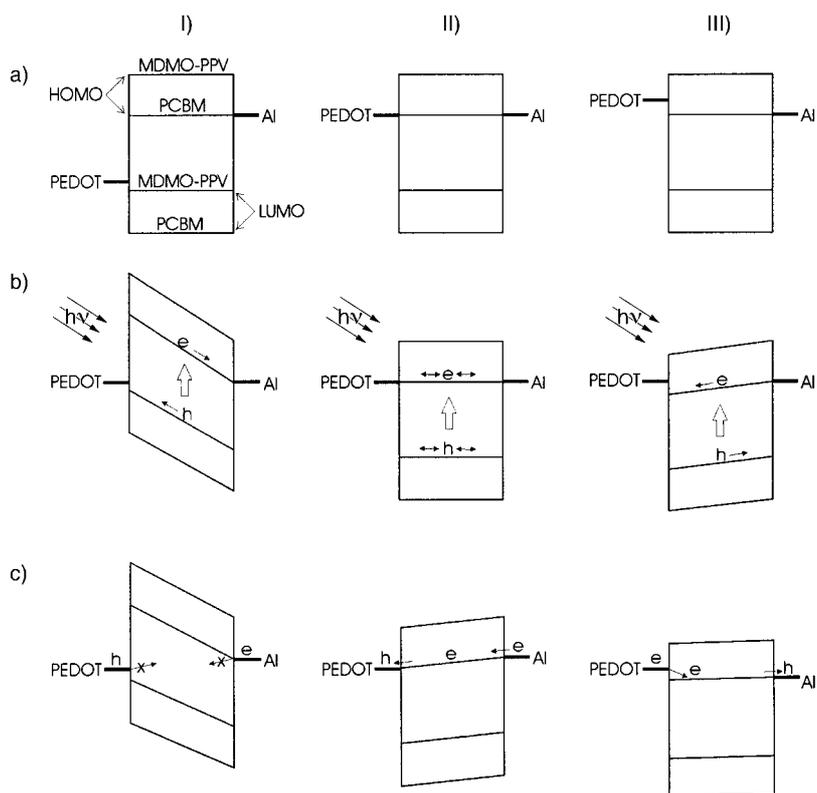
Figure 4. Idealized energy diagrams for OSC devices. I) "Normal" OSC. II) "Zero built-in field" OSC. III) "Inverted" OSC. a) Flat-band situation at compensation voltage (U = V₀). b) Short-circuit conditions under illumination (U = 0 V). c) (Dark) injection; a small external voltage was "applied" in forward direction.

PEDOT. The fact that a "zero built-in-field" OSC is realized when the work function of the PEDOT equals the reduction potential of PCBM demonstrated that the pinning of the cathode (here aluminum) occurs exactly at the LUMO level of the PCBM acceptor. "Inverted" OSCs have been realized for the first time. No pinning of the PEDOT energy levels to the PCBM LUMO level was observed unlike anticipated for the metal cathode. However, the latter is a result of the thermal evaporation process.[4,8] "Inverted" OSCs in general have two technical shortcomings: a) The internal barrier for extraction of photogenerated electrons reduces the short-circuit current, and b) the high series resistance of the undoped PEDOT limits the performance.

Experimental Section

($E_{eq} > E_{ox,PPV}$). For thermodynamic reasons, redox processes between the PEDOT and the adjacent MDMO-PPV layer lead to an exchange of charges, specifically the MDMO-PPV becomes oxidized and the PEDOT reduced until an equilibrium state is reached. This has two important implications: a) Reduction of the PEDOT layer is accompanied by a reduction of E_{eq} and thus ϕ_w, so ultimately the built-in field becomes smaller, and b) even slight oxidation ("doping") of the MDMO-PPV may yield a dramatically higher (dark) conductivity[13] and results in an additional non intensity-dependent current. Both factors lead to the reduction of the OSC performance parameters, and thus explain deviations from the linear dependence in Figure 2 a as well as the "forbidden" range for $E_{eq} > E_{ox,PPV}$ (see above).

Figure 4 allows direct comparison of the different device types. In general, the metal electrode (aluminum) will always provide Ohmic contacts for electrons due to the pinning effect.[4, 8] Electrons will therefore be injected by the Al contact under reverse bias in all devices. Injection of electrons from the PEDOT may occur in OSCs with $V_{bi} \approx 0$ even under forward bias. The injection of holes by the PEDOT will only come into play for highly doped PEDOT, namely in "normal" and "doped" OSCs and for $U > V_0$.

In conclusion, we demonstrated that the controlled adjustment of organic electrodes is a powerful tool to optimize organic solar cells. "Normal" OSCs utilizing commercial PEDOT can be improved by increasing the work function (doping level) of

[1] N. S. Sariciftci, L. Smilowitz, A. J. Heeger, F. Wudl, *Science* **1992**, *258*, 1474.

[2] G. Yu, J. Gao, J. C. Hummelen, F. Wudl, A. J. Heeger, *Science* **1995**, *270*, 1789.

[3] S. E. Shaheen C. J. Brabec, N. S. Sariciftci, F. Padinger, T. Fromherz, J. C. Hummelen, *Appl. Phys. Lett.* **2001**, *78*, 841.

[4] C. J. Brabec, A. Cravino, D. Meissner, N. S. Sariciftci, T. Fromherz, M. T. Rispens, L. Sanchez, J. C. Hummelen, *Adv. Funct. Mater.* **2001**, *11*, 374.

[5] I. H. Campbell, J. D. Kress, R. L. Martin, D. L. Smith, N. N. Barashkov, J. P. Ferraris, *Appl. Phys. Lett.* **1997**, *71*, 3528.

[6] G. Greczynski, W. R. Salaneck, *Appl. Phys. Lett.* **2001**, *79*, 3185.

[7] G. G. Malliaras, J. R. Salem, P. J. Brock, J. C. Scott, *J. Appl. Phys.* **1998**, *84*, 1583.

[8] C. J. Brabec, A. Cravino, D. Meissner, N. S. Sariciftci, M. T. Rispens, L. Sanchez, J. C. Hummelen, T. Fromherz, *Thin Solid Films* **2002**, *403*, 368.

[9] C. M. Heller, I. H. Campbell, D. L. Smith, N. N. Barashkov, J. P. Ferraris, *J. Appl. Phys.* **1997**, *81*, 3227.

[10] M. Gross, D. C. Müller, H.-G. Nothofer, U. Scherf, D. Neher, C. Bräuchle, K. Meerholz, *Nature* **2000**, *405*, 661.

[11] H. Frohne, D. C. Müller, K. Meerholz, *ChemPhysChem* **2002**, *3*, 707.

[12] X. Wei, M. Raikh, Z. V. Vardeny, Y. Yang, D. Moses, *Phys. Rev. B* **1994**, *49*, 17 480.

[13] T. A. Skotheim, *Handbook of Conducting Polymers*, Dekker, New York, NY, **1986**.

[14] E. A. Katz, D. Faiman, S. M. Tuladhar, J. M. Kroon, M. M. Wienk, T. Fromherz, F. Padinger, C. J. Brabec, N. S. Sariciftci, *J. Appl. Phys.* **2001**, *90*, 5343.

Alkyl Monolayer-Passivated Metal – Semiconductor Diodes: Molecular Tunability and Electron Transport

Yong-Jun Liu and Hua-Zhong Yu*[a]

KEYWORDS:

electron transport · mercury · molecular devices · monolayers · silicon semiconductors

The metal – semiconductor (M-S) junction is one of the most important solid-state components in microelectronic integrated circuits. It has been widely used in creating Ohmic contacts, Schottky diodes, and metal – semiconductor field-effect transistors.[1] The fabrication and characterization of metal – semiconductor junctions directly affect the process, characteristics, and performance of these important elements in electronic devices. With the emergence of molecular modification and self-assembly techniques, research activities have been bolstered with the

[a] *Prof. H.-Z. Yu, Dr. Y.-J. Liu*
Department of Chemistry
Simon Fraser University
8888 University Drive, Burnaby, BC, V5A 1S6 (Canada)
Fax: (+ 1) 604-291-3765
E-mail: hzyu@sfu.ca

Supporting information for this article is available on the WWW under http:// www.chemphyschem.org or from the author.

aim of obtaining a full understanding of the formation of metal/molecule/semiconductor junctions and the molecular tunablility of interfaces.[2–6] Silicon is the most popular material in semiconductor devices, therefore, it is extremely important from both fundamental and application perspectives to control the chemical and physical properties of the interfaces between silicon and metals at the molecular level. However, most studies have focused on the oxide-interfaced silicon/molecule/metal junctions prepared by the classical metal deposition technique, namely grafting organosilane monolayers onto naturally oxidized silicon surfaces before the evaporation of metal contacts.[4a, b, 5, 6a, b] The understanding of the exact electrical properties of oxide-free metal/molecule/silicon junctions is still very limited.[3, 4c] In contrast, great progress has been made during the past decade in the fabrication and application of chemically robust Si$-$C bonded monolayers on silicon.[7, 8]

In this Communication, we report how an alkyl monolayer can tune a resistor (such as a direct mercury/silicon contact) to a diode (to a mercury/molecule/silicon junction; Figure 1), and
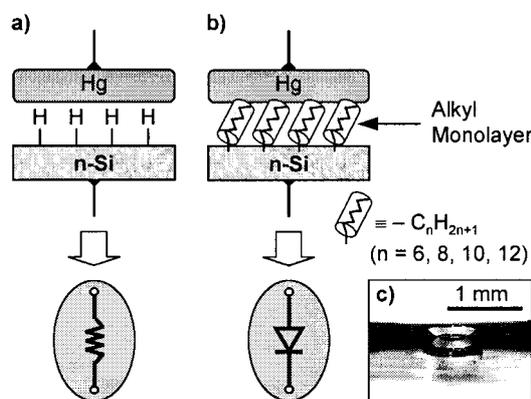

Figure 1. *Schematic illustration of mercury/silicon junctions and their electrical characteristics: a) A direct Hg/H$-$Si (n-type) junction that exhibits Ohmic contact characteristics, that is, it can be represented as a resistor. b) An alkyl monolayer-passivated junction, Hg/C$_n$H$_{2n+1}-$Si (n = 6, 8, 10, 12), that shows rectifying behavior, that is, it can be represented as a diode. c) An optical photograph shows the mercury drop (and its mirror image) in contact with the silicon surface.*

describe how the electron transport correlates to the device performance in these "genuine" metal/molecule/semiconductor junctions. The use of mercury as a "soft" metal contact, initiated 30 years ago,[9] has regained its popularity in the recent studies of the unique electron transport property across metal/mono-layer/metal junctions,[10, 11] and the intriguing electrical behavior of Hg/monolayer/SiO$_x$/p-Si systems.[12] By adapting these innovative experimental approaches, we have constructed easy and reproducible mercury/silicon junctions, in which a mercury drop extruded from a gas-tight syringe was brought into contact with a silicon surface using a custom-made micromanipulator (the contact process and area were monitored by a video microscope using a 40 × objective, Figure 1c). Using this simple and flexible experimental setup to fabricate metal/semiconductor junctions not only overcomes the problems that are often associated with the traditional metal deposition technique (such as changing the surface properties or damaging the molecules preassembled on